Synopsis of the thesis entitled

Nonadiabatic quantum wave-packet dynamics of atom-diatom reactions

to be submitted to the
University of Hyderabad
for the degree of

Doctor of Philosophy

by

B. Jayachander Rao

Supervisor
Prof. Susanta Mahapatra

School of Chemistry
University of Hyderabad
Hyderabad 500 046, INDIA

April 2008

SYNOPSIS

The present thesis entitled '**Nonadiabatic quantum wave packet dynamics of atom-diatom reactions**' deals with treatment of nuclear dynamics in the coupled manifold of electronic states and consists of six chapters. The aim of the thesis is to study the effect of nonadiabatic interactions on dynamical observables *viz.*, the initial state-selected reaction probabilities, integral reaction cross sections and thermal rate constants of H + H_2 (HD) and N (^2D) + H_2 reactions with the aid of a time-dependent wave packet (TDWP) approach. The theoretical results are compared with the available experimental and other theoretical results from the literature.

Chapter 1 provides an overview of the theoretical and experimental advances on the H + H_2 and N(^2D) + H_2 insertion reactions. A brief review on the available literature on H + H_2 and N (^2D) + H_2 reactions is also presented. The hydrogen exchange reaction takes place on the ground electronic state, which is sensitive to the Jahn-Teller (JT) distortions and hence a study of the electronic nonadiabatic effects on the nuclear dynamics of this fundamental reaction has been a major topic theoretical interest for many research groups. The orbital degeneracy of H_3 is split when it is distorted from its equilibrium D_{3h} configuration along its degenerate assymetric stretching and bending modes. The resulting two JT split component potential energy surfaces (PESs) form conical intersections (CIs) (Fig. 1) at the D_{3h} equilibrium configurations of H_3. The effects of CIs on the reactive scattering dynamics and molecular spectroscopy are well studied in lierature in terms of geometric phase (GP) change of adiabatic electronic wavefunction when encircling the CI in a closed loop path or by considering the nonadiabatic coupling explicitly in the formalism. N(^2D) + H_2 reaction is the prototype for the triatomic insertion reactions. This reaction follows an indirect mechanism and is characterized by the presence of deep well on the their PES. The incoming N(^2D) atom attacks the H_2 bond in a T-shaped configuration leading to the formation of a stable NH_2 radical during the cource of the reaction. The ground 1 $^2A''$ and the first excited 2 $^2A'$ elec-

tronic states of NH_2 transform into a degenerate $^2\Pi$ state for linear configurations and thus interact through Renner-Teller (RT) type of vibronic coupling. NH_2 is the first molecular system where RT effects were observed.

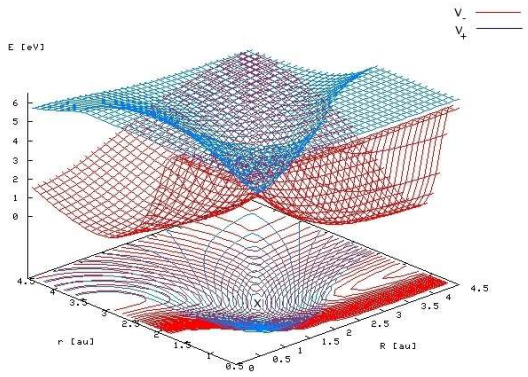

Fig. 1. Adiabatic PESs of ground (shown by red coloured contours) and first excited states (shown by blue coloured contours) of H_3 for D_{3h} geometry. The point of CI is shown by X in the figure.

In chapter 2, the theoretical framework to treat the nuclear dynamics by a TDWP approach is discussed. The body-fixed Jacobi coordinates are utilized to numerically solve the time-dependent Schrödinger equation (TDSE) and to calculate the dynamical obeservables. The nuclear dynamics is treated with a two-state Hamiltonian considering the electronic nonadiabatic coupling effects. The quantum flux operator is represented both in the adiabatic as well as in a diabatic electronic representation. Preparation of the initial WP, its propagation and the final analysis-each of these topics are discussed at length in this chapter. The fast Fourier transform and the discrete variable representation method have been used for the spatial propagation and the chebyshev polynomial expansion method is used for the time propagation of the WP. The reaction probabilities depending on the total angular momentum J are calculated within the coupled-states (CS) approximation. These J-dependent reaction probabilities are utilized to calculate the integral reaction cross sections

and thermal rate constants.

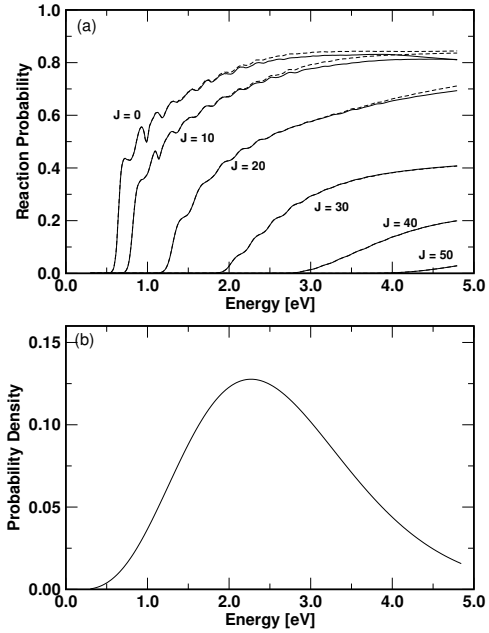

Fig. 2. (a) The reaction probabilites as function of the total energy for H + H_2 ($v = 0, j = 0$) $\rightarrow$ H_2 ($\Sigma v', \Sigma j'$) + H exchange reaction on the DMBE PES for J = 0, 10, 20, 30, 40 and 50. The coupled and uncoupled results are shown by the solid and dashed lines, respectively. (b) The energy distribution of the initial translational (H, H_2) GWP for calculating the above reaction probabilities.

In chapter 3, we present and discuss the H + H_2 (HD) reaction probability results obtained with the formalism outlined in chapter 2. The H + H_2 ($v = 0, j = 0$) $\rightarrow$ H_2 ($\Sigma v', \Sigma j'$) + H reaction probability as a function of total energy E (atom-diatom translational + diatom rovibrational) are plotted in Fig. 2 for a few selected values of the total angular momentum J = 0, 10, 20, 30, 40 and 50 and for $\Omega = 0$. These represent the inital state selected and energy resolved total (summed over all open v' and j' levels of the product H_2 at a given energy) reaction probabilities. The coupled and uncoupled surface results are shown by the solid and dashed lines, respectively. The reaction probabilities are calculated in both cases from the onset of the reaction

to the three-body dissociation limit of H_3. We note here that, this is the first theoretical work of its kind which considers to investigate this exchange reaction over such a wide range of enrgy. It can be seen that the difference between the coupled and uncoupled surface reaction probabilities for a given value of J is nearly zero at low energies. At higher energies near and above the energetic minimum of the seam of CIs (at $\sim$ 2.74 eV) this difference becomes noticeable. However, as J increases, the coupled and uncoupled surface results merge on each other, particularly for $J \geq 30$. The resonance structures seen in the reaction probability curves at low J values gradually disappear as J increases. Beyond $J = 40$ these resonances are not at all seen in the reaction probabilities.

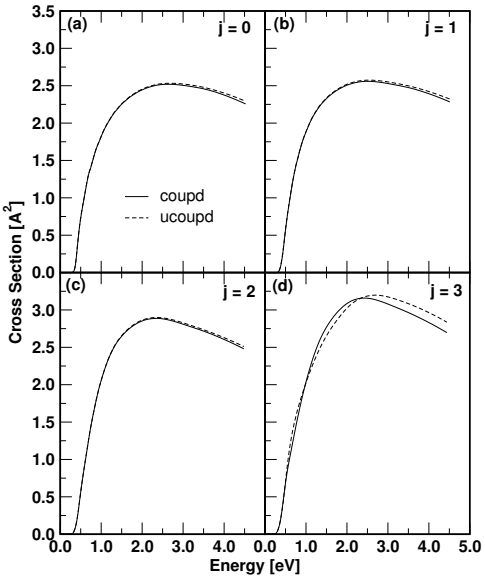

Fig. 3. Initial state-selected integral reaction cross sections of the H + H_2 ($v = 0, j$) as function of the total energy. The cross sections for various j values are indicated in each panel.

The initial state-selected and energy resolved integral reaction cross sections, as a function of the total energy in the H + H_2 collisions are shown in Fig. 3(a-d). The coupled and uncoupled surface results are shown by the full and dashed line

types, respectively, in each panel. The reaction cross sections shown in Fig. 3(a-d) for both the coupled and uncoupled surface situations are obtained with the rotationally excited reagent H_2(j = 0 - 3, in panels (a) - (d), respectively) in the vibrational ground level ($v = 0$). For a given value of j the reaction cross section increases with energy reaching a maximum in the energy range of $\sim$ 2.5 - 2.7 eV and then decreases as the energy increases in both the coupled and uncoupled surface results. The difference between the coupled and the uncoupled-surface results for a given value of j, is small at low collision energies and increases very slightly for j = 0 - 2 beyond the energetic minimum of the seam of CIs. This difference appears to be somewhat larger for $j = 3$.

The thermal rate constants obtanied by statistically averaging over the rotational states j = 0 - 3 are shown in Fig. 4 for H + H_2 ($v = 0$) reaction. The coupled and uncoupled surface results are shown by the full and dashed line types, respectively.

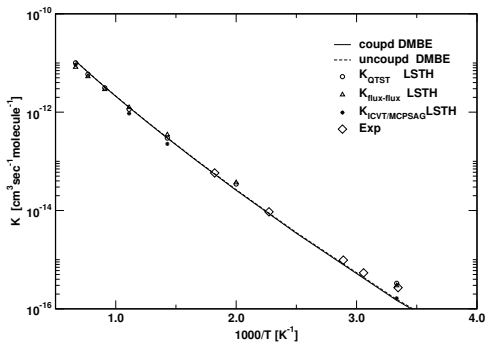

Fig. 4. Arrhenius plot of the Boltzmann averaged (over j = 0 - 3) thermal rate constants for the H + H_2 ($v = 0$) reaction. The coupled and uncoupled surface results are shown by solid and dashed lines, respectively. Points on the diagram represents the results from the literature.

The rate constants values available in the literature are shown by different points on the diagram. The unfilled diamonds represents the experimental points extracted from Table IX of Pack *et al* [J. Chem. Phys., **91**, 974 (1992)]. Fig. 4 reveals that

the difference between the coupled and uncoupled surface results is insiginificant in the reported temperature range of $\sim$ 0 - 1500 K. This drives us to the final point of concluding that the important dynamical observable like the thermal rate constant derived from the microscopic reaction probabilities is insensitive to the nonadiabatic coupling in the H + H_2 reaction dynamics.

In chapter 4, the effect of reagent H_2 rotation and vibration on the dynamics of the H + H_2 reaction is presented and discussed. The effects of electronic nonadiabatic coupling on the dynamics of the most fundamental reaction H + H_2 are also presented. The effect of the reagent rotation and vibration is mainly studied in the present study employing the CS approximation. Intial state-selected and energy resolved reaction probabilities have been reported for reagent, H_2 in its $(v = 0, j = 0 - 10)$ and $(v = 0 - 10, j = 0)$ states, respectively, upto the three-body dissociation limit of H_3 ($\sim$ 4.7 eV). Calculations are performed both with and without surface coupling and the results are compared. The H + H_2 $(v = 0, j = 4)$ reaction probability values as a function of the total energy E (H + H_2 translational + H_2 rovibrational) are plotted in Fig. 5 for few selected values of the total angular momentum $J = 0$, $\Omega = 0$ and $J = 4$, 10, 20, 30, 40 and 50 (indicated in the panel) and for $\Omega = 4$.

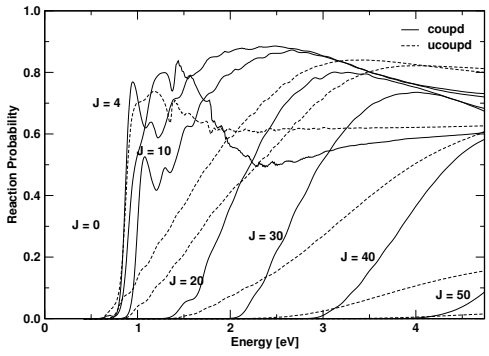

Fig. 5. Total reaction probabilities as a function of the total energy E for the H + H_2 $(v = 0, j = 4)$ reaction on the DMBE PES for the total angular momentum $J = 0$, $\Omega =$

0 and J = 4, 10, 20, 30, 40 and 50 (indicated in the panel) for $\Omega = 4$. The coupled and uncoupled surface results are shown by the solid and dashed lines, respectively.

These represent the initial state-selected and energy resolved total reaction probabilities. The coupled and uncoupled surface results are shown by the solid and dashed lines, respectively. It can be seen from the Fig. 5 that the coupled and uncoupled surfacce results dramatically differ from each other. The reaction threshold in both coupled and uncoupled surface situations shifts to higher energy as J increases. The difference between the coupled and uncoupled surface results increases with increase in J. It can be seen from the Fig. 5 that reactivity increases in the coupled surface situation. It can also be seen from the figure that the uncoupled reaction probability for $J = 50$ is almost zero. The resonance structures are absent in the uncoupled surface results for small values of J.

Initial state-selected and energy resolved integral reaction cross sections, as a function of the total energy in the H + H_2 reaction are shown in Fig. 6(a-k). The coupled and uncoupled surface results are shown by solid and dashed line types, respectively, in each panel. These reaction cross sections shown in Figs. 6(a-k) for both coupled and uncoupled surface situations are obtained with the reagent, H_2 is in its ground vibrational level and j = 0 - 10 levels (indicated in the respective panel). For a given value of j the cross section increases with energy reaching a maximum in the energy range $\sim$ 2.5 - 2.7 eV and then decreases as the energy increases both in coupled and uncoupled surface situations. The difference between the coupled and uncoupled surface results for a given value of j, is small at low collision energies and increases very slightly for j = 0 to 3, at energies beyond the minimum of the seam of CIs. This difference becomes quite pronounced beyond j $\geq$ 3.

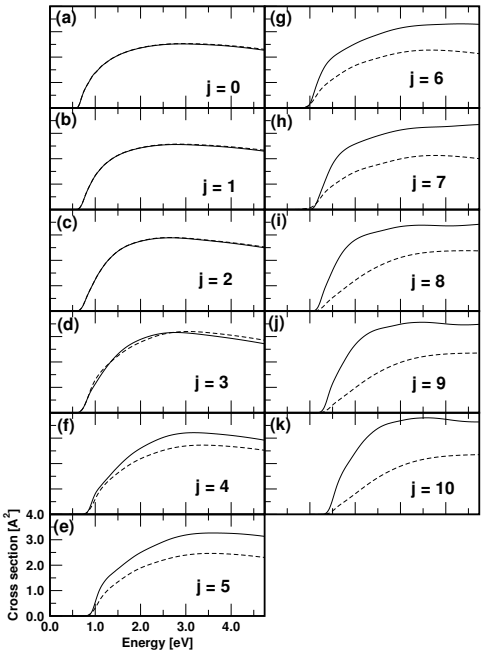

Fig. 6. Initial state-selected integral reaction cross sections of the H + H_2 ($v = 0, j$) as a function of the total energy. The cross sections for various j values are indicated in each panel. The coupled and uncoupled surface results are shown by the solid and dashed lines, respectively

In chapter 5, we study the quantum wave packet dynamics of N(^2D) + H_2 reaction on the recently developed *ab initio* PES of Ho *et al.* [J. Chem. Phys., **119**, 3063 (2003)]. In this study we have ignored the nonadiabatic RT couplings on the dynamics of N (^2D) + H_2 reaction. In this chapter we discuss and present the reaction probability, reaction cross section and thermal rate constant resutls obtained for the N(^2D) + H_2 prototype insertion reaction. All partial wave contributions up to the total angular momentum $J = 55$ were necessary to obtain converged integral reaction cross sections up to a collision energy of 1.0 eV within the CS approximation. The thermal rate constants are calculated from the reaction cross sections and compared with the available experimental and other theoretical results in the literature. We also present and disscuss the typical resonances formed during the course of the reaction and elucidate the insertion mechanism for the product formation. The

vibrational levels supported by the deep well ($\sim$ 5.5 eV) of the 1 $^2A''$ PES of NH_2 are also calculated for the total angular momentum $J = 0$. A statistical analysis of the spacing between the adjacent levels of this energy spectrum is performed and the extent of irregularity in the spectral sequence is assessed.

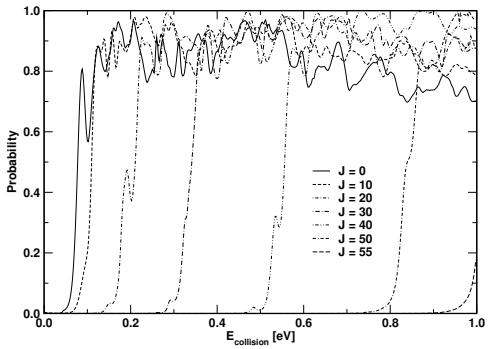

Fig. 7. N (^2D) + H_2 ($v = 0, j = 0$) reaction probability values as function of collision energy are plotted for a few selected values of the total angular momentum $J = 0$, 10, 20, 30, 40, 50 and 55 and for $\Omega = 0$.

The N (^2D) + H_2 ($v = 0, j = 0$) reaction probability values as a function of the collision energy E are plotted in Fig. 7 for a few selected values of the total angular momentum, $J = 0$, 10, 20, 30, 40, 50 and 55 (indicated in the panel) and for Ω =0. It can be seen that the reaction has a threshold, because of the intrensic barrier ($\sim$ 0.08 eV) in the PES, which shifts to the higher energy with increasing contribution from the centrifugal barrier for higher J values. The probabilities show a very sharp rice near the threshold and then oscillate at higher energies for all J values. The oscillations seen in the reaction probability curves of Fig. 7 can be attributed to a large number of quasibound vibrational levels supported by the 1 $^2A''$ PES.

The integral reaction cross section results as a function of collision energy for N (^2D) + H_2 ($v = 0, j$) reaction for four differnet values of j (indicated in the panel) are shown in Fig. 8. The cross section values increase monotonically with increasing collision energy and reach to a plateau at high energies. It can be seen from Fig. 3

that the cross section values increase with the rotational excitations of the reagent diatom. The resonance oscillations also persisit in the cross section results, though they are much weaker compared to those in the reaction probability results.

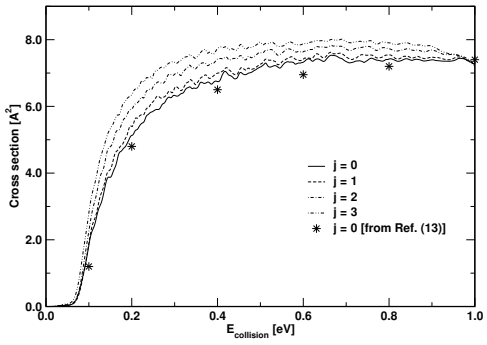

Fig. 8. N (^2D) + H_2 ($v = 0, j$) reaction cross section values as function of collision energy are plotted when the reagent, H_2 is in $j = 0$ - 3 states as indicated in the panel.

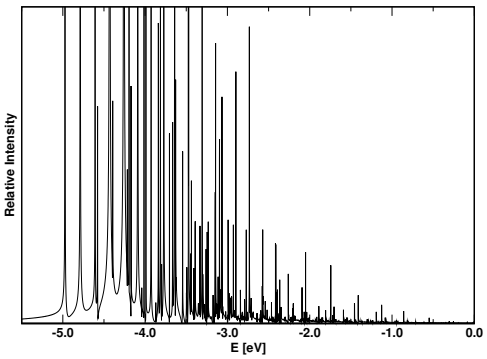

Fig. 9. A typical vibrational energy level spectrum of NH_2, computed with the GWP No. 4 (cf., Table II). The intensity is plotted in arbitary units as a function of energy of the vibrational levels. The zero of energy corresponds to asymptotically separated N + H_2 reactants.

A typical vibrational energy level spectrum of NH_2 is shown in Fig. 9 for the total

angular momentum $J = 0$. The intensity in arbitary units is plotted as a function of the energy of the vibrational levels of the 1 $^2A''$ electronic state. The peaks in the spectrum correspond to the vibrational energy levels of the NH_2 radical and energy corresponding to the peak maximum represents the vibrational energy eigenvalues.

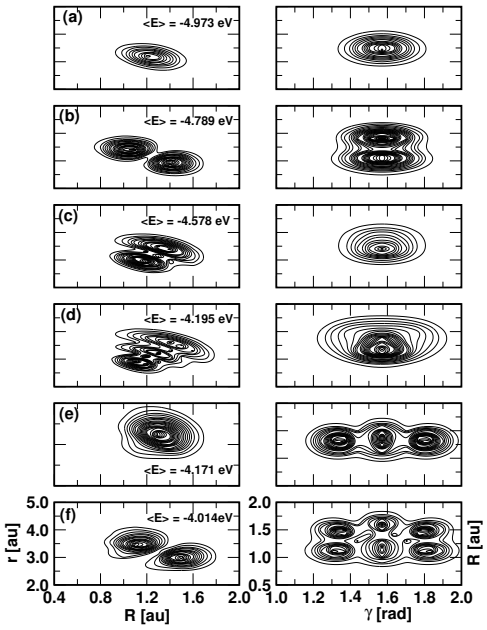

Fig. 10. Probability density contours of the eigenfunctions of the low-lying vibrational levels of NH_2. The contours are plotted in the (R, r) plane averaged over γ (left column) and (γ, R) plane averaged over r (right column), to clearly reveal the nodal pattern in them.

The nature of the peaks implies that the levels are of bound type. It can be seen from Fig. 9 that at low energies near the bottom of the well, resolved peaks are obtained. The number of peaks in the spectrum increases significantly with an increase in energy. The energetic minimum of the well of the 1 $^2A''$ PES occurs at $\sim$ 5.5 eV for the C_{2v} geometry of NH_2. It can be seen that the 0 - 0 line in the spectrum of Fig. 9 occurs close to this energy. Approximately 400 vibrational levels

are calculated by varying the location of the initial WP in the well region of the 1 $^2A''$ PES.

The eigenfunctions of these vibrational levels are calculated and their probability density ($|\Psi(E)|^2$) contours are plotted in Fig. 10 (a-f) in the (R, r) and (γ, R) planes averaged over γ and r, respectively. The eigenfunctions reveal both local and hypersperical mode type of behavior and exhibit nodal progression along R, r and along the polar angle, Φ ($= \tan^-1\ (\frac{r}{R})$), respectively. In order to have an insight of the extent of coupling between the three degrees of freedom and the observed complex pattern of the vibrational wavefunctions at higher energies we examine the calculated ~ 400 vibrational levels for shortrange correlations by analyzing the nearest neighbour spacing distribution (NNSD).

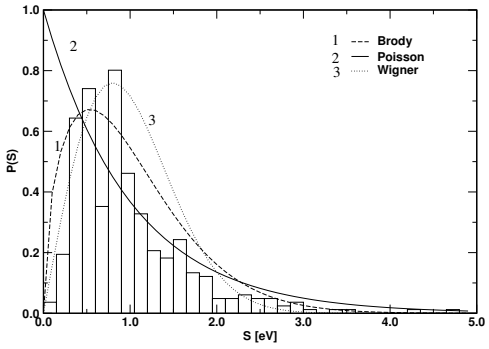

Fig. 11. The nearest neighbor spacing distribution $P(s)$ as a function of the spacing s between energy levels derived from the unfolded bound state spectrum of NH_2 given in Fig. 8. Poisson (curve 1) and Wigner (curve 2) distributions correspond to the regular and irregular limits, respectively. The best fit of the histogram to the Brody distribution with $q = 0.7$ (see text) is included in the figure by curve 3.

Prior to the application of this statistical analysis, the energy spectrum is unfolded. This makes the average density of levels uniform over the entire energy range and removes the irrelevent secular variations of the spacing keeping the fluctuating variations unaffected. These unfolded energy values are used to estimate the corre-

lation between the adjacent energy levels by analyzing the NNSD. The summarizing remarks including the future directions are provied in chapter 6. In Appendix 1, a theoretical study of the JT CIs in the 3p (E') and 3d (E'') Rydberg electronic states of triatomic hydrogen is undertaken. In this chapter, we present and discuss the static and dynamic aspects of the JT interactions in the two Rydberg electronic states of H_3 mentioned above. The static aspects are discussed based on recent *ab initio* quantum chemistry results, and the dynamics aspects are examined in terms of the vibronic spectra and nonradiative decay behavior of these degenerate electronic states. The adiabatic PESs of these electronic states are derived from extensive *ab initio* calculations. The calculated adiabatic PESs are diabatized. The nuclear dynamics on the resulting conically intersecting manifold of electronic states is studied by a time-dependent WP approach. Calculations are performed both for the uncoupled and coupled state situations in order to understand the importance of nonadiabatic interactions due to the JT CIs in these excited Rydberg electronic states. Our findings reveal that the nonadiabatic coupling effects in these Rydberg electronic manifold of H_3 are much milder than those found in case of its 2p (E') ground electronic manifold. Comparing the two Rydberg electronic states, the nonadiabatic effects are sligtly stronger in case of 3p (E') electronic manifold.